Journal of Agricultural Engineering

https://www.agroengineering.org/

Design and experimental study of bionic digging shovel based on vole's front middle toe

Hanhao Wang, Yaoming Li, Ying Wu, Kuizhou Ji, Yanbin Liu

School of Agricultural Engineering, Jiangsu University, Zhenjiang, China

Corresponding author: Yaoming Li, School of Agricultural Engineering, Jiangsu University, Zhenjiang 212013, China. E-mail: ymli@ujs.edu.cn

Please cite this article as doi: 10.4081/jae.2025.1831

Submitted: 5 May 2025
Accepted: 26 July 2025

Design and experimental study of bionic digging shovel based on vole's front middle toe

Hanhao Wang, Yaoming Li, Ying Wu, Kuizhou Ji, Yanbin Liu

School of Agricultural Engineering, Jiangsu University, Zhenjiang, China

Corresponding author: Yaoming Li, School of Agricultural Engineering, Jiangsu University, Zhenjiang 212013, China. E-mail: ymli@ujs.edu.cn

Contributions: all the authors made a substantive intellectual contribution, read and approved the final version of the manuscript and agreed to be accountable for all aspects of the work.

Conflict of interest: the authors declare no competing interests, and all authors confirm accuracy.

Funding: The work was supported by the Key Projects of the Ministry of Agriculture and Rural Affairs (NK202216050102) and Zhenjiang Key R&D Project (SNY20220130032).

Abstract

To reduce the drag encountered by the potato harvester during excavation in wet soil, a bionic digging shovel was designed based on the vole's front middle toe. By using MATLAB software to extract and fit the information of the contour curve of the vole's front middle toe, the bionic digging shovel model was designed and established. A comparative experiment was conducted on the vole-imitating digging shovel, Gryllotalpa-imitating digging shovel, and common digging shovel in EDEM software, to verify that the vole-imitating digging shovel has drag reduction capability. Through single- and multi-factor simulation analysis, the structural and operational parameters of the vole-imitating digging shovel were optimized. The excavation drag of three types of shovels was compared through field experiments, and the correctness of the simulation results was verified. The results show that the optimal parameter combinations of the vole-imitating digging shovel, i.e., a single shovel width of 135 mm, an entry angle of 20°, and a forward speed of 0.5 m/s. Under the same working conditions, the vole-imitating digging shovel has a better drag reduction effect and a higher soil breakage

efficiency than the other two shovels.

Key words: potato harvester; bionic digging shovel; vole's front middle toe; drag reduction; discrete element simulation; field experiment.

Introduction

Potato is an herbaceous tuberous asexual reproductive crop with high nutritional value, which can be used not only as food and vegetable, but also in pharmaceutical, industrial and healthcare sectors (Dou *et al.*, 2019; Wu *et al.*, 2023). Compared with other crops, potato has growth characteristics such as barrenness, cold and drought resistance, and can be planted in remote and alpine areas without the constraints of arable land resources, so potato has amazing development potential and considerable economic benefits (Zihui *et al.*, 2019; Tunio *et al.*, 2020). Digging shovel as the core working parts in the digging process, its main function is to dig up the soil and potato under a certain digging depth and transport them backward, at the same time, the digging shovel also needs to play a certain role in loosening the soil. Due to the relatively decentralized distribution of potato cultivation, the excavation resistance of digging shovels varies under different soil environments. Under the wet soil environment in some areas, due to the water absorption, adsorption and strong plasticity of the wet soil, the soil is easy to stick on the shovel surface when digging, resulting in congestion on the shovel surface, so the potato harvester is more prone to excessive digging resistance when the shovel is harvesting in the area of high soil moisture content. The effect of high resistance can lead to low harvesting efficiency, high power consumption of power equipment and accelerated wear and tear of the digging shovel. Therefore, further research is needed on how to reduce the amount of wet soil on digging shovels in humid working environments and lower the resistance they encounter.

In order to reduce the digging resistance, reduce the digging power consumption and improve the digging performance, numerous scholars have made innovations in the structure and configuration of excavating devices. Gholamhossein *et al.* (2010). designed a vibratory subsoiler from the principle of vibrating drag reduction, and conducted a series of tests in the field, the test results showed that adding vibration device in the implement can reduce forward resistance. The increase in vibration frequency will increase the forward resistance of

the subsoiler, while the machine will obtain the optimum vibrating subsoiling frequency to minimize the power consumption of the subsoiler. Sun *et al*. (2018). designed a potato digger with waste film recollection that features a split plate combination shovel, differing from the traditional integrated flat shovel. The gaps between the shovels allow soil particles and weeds to pass through smoothly, thereby reducing digging resistance. Bayboboev *et al.* (2022). designed a potato harvester with combined vibration of shovel and sieve for the characteristics of potato cultivation in hilly mountainous areas. Subsequently, fixed digging and vibrating digging were tested in comparison, and the results showed that the vibrating potato digger could improve the digging efficiency and reduce the damage to potato tubers.

Innovations in structure and configuration types will lead to an overall increase in the complexity of the excavation device, thereby reducing its stability in complex operational environments. At the same time, soil animals in nature possess body structures that can effectively reduce digging resistance, providing a natural model and optimization basis for the design of reduced resistance in agricultural machinery's soil-contact components. In recent years, many scholars have applied bionic technology to the research and design of potato digging shovels, resulting in objective performance improvements. Shi *et al*. (2014, 2018). designed a bionic potato digging shovel based on the profile of gryllotalpa claws. Simulation results indicate that this bionic digging shovel can shear and break the lifted soil, gradually reducing resistance in both horizontal and vertical directions. Li *et al*. (2020). inspired by pangolin scales and designed a bionic digging shovel with a surface treatment aimed at reducing adhesion, effectively minimizing the adhesion of soil on the shovel surface during excavation. Aiming at the problems of excessive resistance, poor soil breaking performance and significant amount of wet soil on the shovel surface when digging pseudoginseng seedlings, Chongchong *et al.* (2020). designed a digging shovel imitating the middle toe of the pangolin's forepaw, and applied the scale property in the design of the shovel surface material. The analyses of the simulation experiments showed that the shovel had better resistance reduction and soil crushing performance. Zhang *et al*. (2022). collected point cloud data of a wild boar head's three-dimensional model, determined the structural curve of the bionic shovel, and designed a bionic digging shovel whose convex structure can effectively promote the flow of soil particles. Yu *et al*. (2022). researched mole toes and designed a bionic potato

digging shovel. Field tests indicated that this bionic digging shovel was more effective than a conventional shovel in breaking up the soil. Chengmao *et al.* (2023). designed a bionic digging shovel based on the soil stress analysis of Moore-Coulomb theory, using the shark dorsal fin structure as the projecting structure of the digging shovel, and concluded that this projecting structure is more likely to make the soil reach the rupture state, which is able to reduce the digging resistance through the discrete element simulation analysis.

There are numerous issues in the existing research on bionic potato digging shovels, such as difficulties in processing making them unsuitable for practical production, remaining solely in theoretical research without experimental validation, and unreasonable selection of bionic model. Therefore, this study selects the vole, which has long lived in the soil, as the bionic model, applying its claw toe contour curves to the design of the digging shovel. The goal is to develop a potato digging shovel with a simple structure that is easy to process and has low digging resistance. This research involves the design of the bionic digging shovel through theoretical studies and simulation analysis, and its effectiveness was validated through comparative experiments with existing research findings.

Materials and Methods

Design of the bionic vole-imitating digging shovel

Voles, belonging to the hamster family, are generally 10-15 cm in length, and are widely distributed, moisture-loving, burrowing 5-30 cm below ground, and feeding on the roots and stems of underground plants. Voles need to dig up a lot of soil when foraging and nesting, and over time their front paws have evolved a strong digging ability. Voles have a total of five toes on their front paws, with the second, third, fourth and fifth toes having a digging function. By comparing the index of power arm coefficient of farmland rodents, it was found that the high-power arm coefficient of voles indicates the high digging efficiency of voles. The inner contour curve of the vole's claw toes has a complex variable curvature characteristic, which makes the internal pressure of the soil fluctuate repeatedly and thus facilitates soil crushing. By comparing the fluctuation of the contour curve of each paw and toe of the vole, it was found that the fluctuation of the curvature trend line of the inner contour curve of the front middle toe was the most obvious, so this paper takes the middle toe of the front paw of the common

vole as a bionic object (Wang *et al.*, 2019; Wan *et al.*, 2022).

This study takes the eastern meadow mouse as a bionic model, as this species is widely distributed in northeast China, north China, and the plains of the middle and lower Yangtze River, and its habitat completely overlaps with the potato harvesting environment of this research. Researchers legally and compliantly obtained specimens of the eastern meadow mouse through online channels, subsequently using scissors to cut off the middle toe from its front paw and placing it on a black background cloth, capturing a vertical photograph of the lateral contour of the middle toe with a camera (Figure 1).

In order to observe the contour curve of the vole's paw toes, tweezers were used to remove the parts of the vole's paw toes that were not related to excavation, and the main soil-touching parts were retained for magnification, and the pictures were imported into MATLAB (MathWorks, 2020a) for image processing. Firstly, the rgb2gray command is used to greyscale the image to remove the color information of the original image and highlight the target area; then the imerode command is used to erode the greyscale image to eliminate the boundary points of the image and remove the burrs and small bumps; use the imdilate command to expand the corrosion image, so that the image corrosion is too much to fill the region, the picture outline is smoother and more complete; and then use the in2bw command to the expansion of the image binarization process, to remove redundant data information, highlighting the target contour; and finally use the edge function to detect the edge of the contour and obtain the contour curves (Figure 2 A-F). The processed contour curves were extracted in pixel coordinates using MATLAB and plotted in a pixel coordinate system (Figure 2G).

The least squares method was used in polynomial fitting of the point data obtained for the inner and outer contour curves, and in order to ensure the accuracy of the fitting, the order of the equations was continuously carried out to make the fitting results coincide with the contour curves. Finally, the least squares six times polynomial fitting method was determined, and the function expression equations were obtained after fitting the inner and outer contour curves of the vole's toe, respectively. Among them, the functional expression equation after fitting the inner contour curve is:

$$y_1 = a_1x^6 + b_1x^5 + c_1x^4 + d_1x^3 + e_1x^2 + f_1x + g_1 \quad \text{(Eq. 1)}$$

The values of the coefficients in Eq. (1) are respectively: a_1=-1.244e-11 , b_1=3.43e-8 , c_1=-3.095e-5 , d_1=0.02349 , e_1=-7.88 , f_1=1399 , g_1=-1.027e5 , x∈(283, 595), the goodness of fit R^2 = 0.9806 indicates that the equation is fitted with high accuracy.

The functional expression equation after fitting the outer contour curve is:

$$y_2 = a_2x^6 + b_2x^5 + c_2x^4 + d_2x^3 + e_2x^2 + f_2x + g_2 \quad \text{(Eq. 2)}$$

The values of the coefficients in Equation (2) are respectively: a_2=-1.058e-14 , b_2=6.712e-11 , c_2=-1.219e-7 , d_2=0.0001017 , e_2=-0.04571 , f_2=11.32 , g_2=-893.5 , x∈(166, 595), the goodness of fit R^2 = 0.9991 indicates that the equation is fitted with high accuracy.

The inner and outer contour lines of the mid tow of the field mouse after fitting are shown in Figure 2H. These contour lines will be used for the design of the side profile of the bionic digging shovel.

The configuration of the bionic digging shovel is consistent with that of the common digging shovel, both forming the digging device of the potato harvester through a parallel installation method. During harvesting process, both the bionic digging shovel and the common digging shovel are inserted into the soil at a certain angle, with the shovel tip needing to reach a position deeper than that of the potatoes, ensuring a clean extraction without damaging the potatoes. The distinction between the bionic digging shovel and the common digging shovel lies in their side profiles, where the common digging shovel has a flat plate shape, whereas the profile of the bionic digging shovel is designed and modeled based on the fitting curve calculated earlier. The fitted inner contour curve is applied to the design of the upper shovel surface, the fitted outer contour curve is applied to the design of the lower shovel surface, and the fitted contour curve equations are imported into SolidWorks (Dassault Systèmes, 2022) to model the bionic shovel. The growing depth of the potato in the test field is 150 mm, and the digging depth is set at 160 mm in consideration of the fact that it can be dug up cleanly and without damaging the potato. Since the angle of the digging shovel is generally between 10° and 25° (Yang and Shang, 2012), the angle of the digging shovel was set at 20°, and the length of the digging shovel was calculated to be 350 mm. Thus, the design of the bionic vole-imitating digging shovel has been completed.

Simulation design

Simulation experiment design for structural verification of vole-imitating digging shovels

The interaction process between soil and digging shovel is the main research object of this paper, in order to be able to use EDEM (EDEM Ltd., 2020) to effectively simulate the actual digging and harvesting process of potato harvester, it is necessary to establish a soil particle model that fits with the reality (Wang *et al.*, 2022).

The contact model between particles can be used to describe the interaction between particles after contact, and the Hertz-Mindlin with bonding contact model is selected because there is a certain adhesion relationship between the soils (Gao *et al*., 2024; Liang *et al*., 2023). The relevant simulation parameters of soil particles and digging shovel model were determined by referring to the relevant existing research results (Li *et al*., 2019; Qishuo *et al*., 2017; Xianliang *et al*., 2017; Yan *et al*., 2015; Yang *et al*., 2024). Table 1 shows the physical parameters and contact parameters of soil and digging shovel. A soil trench with a length of 2300 mm, a width of 800 mm and a height of 400 mm was modelled in EDEM, which meets the requirements of digging width and digging depth at the same time. In order to restore the actual soil environment, soil particles are generated in three stages. Firstly, a certain number of soil particles are generated to cover the bottom of the trench to form the subsoil; after the subsoil particles are accumulated and stabilized by gravity, a certain number of soil particles are generated above it to form the intermediate soil; after the intermediate soil is accumulated and stabilized by gravity, a certain number of soil particles are generated above it to form the upper soil. Among them, the depth range of the middle layer of soil is consistent with the depth range of potato growth.

In order to verify the drag reduction effect of vole-imitating digging shovels，the shovel will be compared with the digging resistance of the gryllotalpa-imitating digging shovel and the widely used common digging shovel. The gryllotalpa-imitating digging shovel was developed by Shi *et al*. (2014). which is a representative research achievement in the biomimicry of potato digging shovels in China; however, the shovel has not been processed into a physical entity and subjected to field experiments. This study has conducted modeling restoration and

prototype processing of the gryllotalpa-imitating digging shovel, complementing previous research results while also using it as one of the comparative objects for the vole-imitating digging shovel.

The three types of digging shovels were modelled using SolidWorks according to the parameters of 350 mm for the length of a single shovel and 165 mm for the width of a single shovel. Three models of digging shovels were saved as IGS format and imported into EDEM, and only the process of digging soil with a single digging shovel was simulated to improve efficiency. The angle of the digging shovel was set to 20°, the forward speed was set to 0.5 m/s, the digging depth was set to 160 mm according to the growth depth of the potato, the forward direction was the X-axis direction, and the total time of the simulation was set to 3.5 s, and the time step was 20%.

The drag reduction performance of the bionic digging shovel is shown by the drag reduction ratio, which is calculated by the following equation:

$$\eta = \frac{F_v - F_u}{F_v} \quad \text{(Eq. 3)}$$

One-factor simulation experimental design

In order to explore the effects of single shovel width, angle of entry and forward speed of the digging shovel on the digging resistance, the three factors above are taken as test factors, and the resistance generated by a single imitation vole digging shovel when digging is taken as test indexes, and the effects of these three factors on the digging resistance are explored through one-factor simulation analysis.

The determination of the single shovel width takes into account both the limit width of the wire cutting of the processing factory and the excavation width of the prototype. Finally, four levels were selected: 105 mm, 135 mm, 165 mm, and 195 mm. The angle of entry into the soil is determined according to the adjustable range of the digging device of the experimental prototype, which has an adjustable angle range of 5° to 30°. In this study, four data points of 10°, 15°, 20°, and 25° were selected for comparative research. The forward speeds are determined based on the four rated operational gear positions of the experimental prototype. The corresponding forward speeds for these four positions are 0.5 m/s, 0.8 m/s, 1.1 m/s, and

1.4 m/s. The one-factor simulation test arrangement is shown in Table 2.

Multifactorial simulation experimental design

In order to further investigate the effects of the interaction between the single shovel width, the angle of entry and the forward speed on the digging resistance, the Box-Behnken Design response surface test in Design Expert software (Stat-Ease, Inc., 2020) was used to optimize the single shovel width A, the forward speed B and the angle of entry C, and the digging resistance generated by the vole-imitating digging shovel was used as the test index. A total of 17 groups of simulation tests with three factors and three levels were carried out to seek the optimal parameter combinations of the vole-imitating digging shovel. The width of the single shovel is 105 mm, 135 mm and 165 mm, the forward speed is 0.5 m/s, 0.8 m/s and 1.1 m/s, and the angle of entry is 15 °, 20 ° and 25 ° respectively.

Field experiment design

Experimental device

The prototype machine used in this test is a self-propelled potato harvester developed by School of Agricultural Engineering, Jiangsu University. The harvester consists of digging, separating and conveying devices, with a harvesting width of 1200 mm, suitable for two-row harvesting operations. This prototype is particularly applicable for the harvesting of vegetable potatoes in Shandong, China. The excavated potatoes will be spread out in the field, followed by manual picking. Therefore, the working efficiency of the machine accounts a relatively low weight in the overall operational performance of the entire system.

The resistance test required for this test uses the digital display push-pull tester and S-type external tension transducer produced by Edelberg Instruments Co., Ltd, with a range of 0~5000 N and a resolution of 0.001 N. The mounting base of the tension transducer is welded to the test prototype, and one end of the tension transducer is fixed by a pin with the transducer mounting base welded to the excavation device, and the other end is fixed by a pin with the transducer mounting base welded to the frame. One end of the tension sensor is fixed to the sensor mounting base welded to the excavator through a pin, and the other end is fixed to the sensor mounting base welded to the frame through a pin. On each side of the prototype

installed a tension sensor, the two tension sensors to determine the sum of the tension is the total resistance of the digging shovel in the working process. Figure 3 shows the schematic diagram of the installation of the tension sensor and three types of digging shovels on the test prototype.

In order to verify the drag reduction performance and soil breaking ability of the bionic digging shovel in the actual harvesting process, the vole-imitating digging shovel designed in this paper was processed according to the optimal parameters after simulation optimization, and at the same time, the bionic gryllotalpa-imitating digging shovel and the common digging shovel were processed according to the same digging shovel width and length for the comparative test. The material of the digging shovel is 65Mn, and in order to ensure the high hardness of the digging shovel, the tip and the edge of the shovel are heat-treated during the machining process. The width of the shovels is 135 mm, the distance between neighboring shovels is 17 mm when mounted on the shovel frame, and the number of each shovel is 8.

Experimental design

In order to verify the drag reduction performance of the vole-imitating digging shovels in the actual harvesting process, three types of digging shovels were tested for comparative field digging resistance with the shape of digging shovels, the angle of entering the soil and the speed of advancing as the variables, and the value of resistance in the horizontal direction as the test indexes. The digging depth was uniformly set at 160 mm, and each type of digging blade was tested at 15°, 20° and 25° entry angles at forward speeds of 0.5, 0.8 and 1.1 m/s, respectively.

Results and Discussion

Analysis of simulation results

Analysis of vole-imitating digging shovels structural verification simulation

By using the post-processing tool in EDEM software to extract the resistance values in the X-axis direction of three types of digging shovels, the resistance values in the time period of 0~2.3 s were taken and fitted into the curve shown in Figure 4. During the time period of 0~1 s, the digging shovel gradually enters the soil and is in the stage of entering the soil, and the

digging resistance gradually increases, and during the time period of 1~2.3 s, the digging shovel is in the stage of stable digging, and the digging resistance fluctuates to a certain extent, but the trend of change is relatively smooth. After 2.3 s the digging shovel was excluded from the analysis because it was in the phase of leaving the soil and there was a build-up of soil and a surge in excavation resistance due to the length limitations of the soil particle bed model.

Figure 4 also shows that the resistance of the vole-imitating digging shovel is smaller than that of the common digging shovel and the gryllotalpa-imitating digging shovel, and the fluctuation amplitude of the resulting resistance curve is larger. This is due to the fact that the curvature arc of the shovel surface of the vole-imitating digging shovel is the largest, the speed change of soil movement in the shovel surface is larger, and the distribution domain of the horizontal direction force is wider. Taking the resistance value in the stable digging time period of 1~2.3s, the average resistance of a single vole-imitating digging shovel is calculated to be 157.64 N, the average resistance of a single gryllotalpa-imitating digging shovel is calculated to be 176.87 N, and the average resistance of a single common digging shovel is calculated to be 201.18 N. The calculated drag reduction rate of the vole-imitating digging shovel is 21.64%, and the drag reduction rate of the gryllotalpa-imitating digging shovel is 12.08%. It can be seen that the bionic digging shovel has a certain drag reduction effect, and the drag reduction effect of the vole-imitating digging shovel is better than that of the gryllotalpa-imitating digging shovel.

In order to analyze the motion state of soil particles on the shovel surface when digging with common digging shovels, gryllotalpa-imitating digging shovels and vole-imitating digging shovels, the motion state diagrams of soil particles on the shovel surface when the three types of digging shovels were just entering the soil (0.160s), gradually entering the soil (0.640s) and completely entering the soil (1.300s) were intercepted as shown in Figure 5.

At 0.16 s, the shovel tips of the three types of digging shovels had just touched the soil, at which time there was no obvious change in the soil above the common digging shovel and the gryllotalpa-imitating digging shovel, while the soil above the vole-imitating digging shovel had already shown some extruded deformation. At 0.64 s, all three types of digging shovels were in the stage of gradually entering the soil, and the soil particles moved backward along the shovel face, at this time, there was an obvious bending phenomenon of the soil particles above the vole-imitating digging shovel, which was due to the bending arc of the shovel face of the

vole-imitating digging shovel. At 1.3 s, all three types of digging shovels were at the stage of complete soil penetration, at which time the surface and intermediate soil particles were still in a continuous state behind the common digging shovels and the gryllotalpa-imitating digging shovels; behind the vole-imitating digging shovels, the dispersing effect of the surface and intermediate soil particles was obvious, and a large number of intermediate soil particles were mixed with the bottom soil particles. The reason for this phenomenon is that the soil in the middle of the shovel slows down under the action of the arc of the shovel surface of the vole-imitating digging shovel, while the soil in the front of the shovel still moves backward at a faster speed, resulting in the soil at the back of the shovel being squeezed continuously, thus breaking up, so that it can be seen that vole-imitating digging shovel can be better prevented from congestion due to the bonding of the soil.

In order to analyze the velocity change of soil particles on the shovel surface of common digging shovels, vole-imitating digging shovels and gryllotalpa-imitating digging shovels, the cloud diagrams of soil velocity change during digging of the three types of digging shovels at the moment of 0.6 s were intercepted as shown in Figure 6.

Soil particles move fastest on the upper surface of the vole-imitating digging shovel, and these soil particles drive the surface soil particles away from the shovel surface, causing the soil above the digging shovel to be crushed backward and fall from the back of the digging shovel. The first soil particles that start to move on the common digging shovel and the gryllotalpa-imitating digging shovel cannot effectively drive the rest of the soil particles to move, which causes the soil to be difficult to break up and the movement speed is slower.

Analysis of one-factor simulation

In Figure 7 the effect pattern of different factors on the digging resistance of the vole imitating digging shovel is shown.

From Figure 7A it can be seen that at the same angle of entry and forward speed, when the width of the digging shovel is 105 mm, the resistance generated during digging is the smallest. The larger the width of the digging shovel, the greater the digging resistance generated by the vole imitating digging shovel when digging, because as the width of the digging shovel increases, the more soil the digging shovel lifts up, the greater the pressure brought by the soil

that the shovel surface bears, which leads to an increase in the digging resistance.

From Figure 7B, it can be seen that at the same width and forward speed, the digging resistance is larger when the angle of entry is 10°, because the entry performance is poorer when the angle of entry is too small. When the angle of entry is between 15° and 25°, the distribution of digging resistance curve is more concentrated. When the angle of entry is 15°, 20° and 25°, the average resistance is 164.95 N, 157.64 N and 163.03 N, respectively, and it can be seen that the digging shovel produces the smallest resistance under the angle of entry of 20°.

From Figure 7C, it can be seen that at the same angle of entry and width, when the forward speed is 0.5 m/s, the vole-imitating digging shovel produces the smallest resistance when digging. The greater the forward speed, the greater the resistance generated by the vole-imitating digging shovel, the reason is that with the increase of the forward speed of the digging shovel, the more soil rises per unit time of the digging shovel, which makes the amount of soil disturbance increase, resulting in the increasing resistance of digging.

In summary, the digging resistance is lower when the single shovel width of the digging shovel is in the range of 105~165 mm, the angle of entry is in the range of 15°~25°, and the forward speed is in the range of 0.5~1.1 m/s.

Analysis of multifactorial simulation

The results after the multifactor simulation test are shown in Table 3. Quadratic polynomial regression was fitted to the test results using Design-Expert software to establish the second-order regression model for the single shovel width, the angle of entry and the forward speed of the digging shovel, and the analysis of variance was performed on the established model. The results of the analysis of variance for the digging resistance produced by the vole-imitating digging shovel when digging was shown in Table 4. The F-value of this regression model is 36.07, $p<0.0001$, indicating that the regression model is extremely significant; the p-value of the misfit term is greater than 0.05, with a non-significant effect, indicating that the regression equations fitted by the model are in line with the reality, with a good degree of fit. The effect of influence factor B (forward speed) on digging resistance is very significant, the effect of influence factor A (single shovel width) on digging resistance is significant, and the effect of

influence factor C (angle of entry) on digging resistance is not significant. The order of influence of each factor on excavation resistance was B (forward speed) > A (single shovel width) > C (angle of entry). The regression equation of digging resistance with significant factors was obtained by eliminating the insignificant terms in the analysis of variance as:

$$\textbf{\textit{Digging resistance}} = 425.53 + 20.78A + 48.43B - 7.12C - 2.54AB - 2.96AC - 6.26BC + 104.24A^2 - 2.41B^2 + 99.58C^2 \quad \text{(Eq. 4)}$$

The response surface method is used to analyze the effect of the interaction of two-factor on the digging resistance by fixing one factor at an intermediate level in turn and analyzing the effect of the other two factors on the digging resistance. Figure 8 shows the response surface diagram of different two-factor interactions.

When the width of the digging shovel is certain, with the increase of the forward speed, the digging resistance is always increasing; with the increase of the angle of entry, the digging resistance is decreasing and then increasing; when the forward speed of the digging shovel is 0.5 m/s, and the angle of entry is 20°, the digging resistance is the smallest. When the digging shovel forward speed is certain, with the increase of the single shovel width, the digging resistance is first reduced and then increased; with the increase of the angle of entry, the digging resistance is also first reduced and then increased; when the digging shovel single shovel width of 135 mm, the forward speed of 0.5 m/s, the digging resistance is the smallest. When the angle of the digging shovel into the soil is certain, with the increase of the width of the single shovel, the digging resistance is first reduced and then increased; with the increase of the forward speed, the digging resistance has been increased; when the single shovel width of the digging shovel is 135 mm and the forward speed is 0.5 m/s, the digging resistance is the smallest.

Through the analysis of part of the structure and working parameters of the imitation vole digging shovel, in order to obtain the optimal parameter combination of the vole imitating digging shovel with less digging resistance, the parameter optimization function in the Design Expert software is used to optimize and solve the simulation results, and the optimization constraints are determined by combining with the boundary conditions of the influencing factors, and the constraints are:

$$\begin{cases} minY(A,B,C) \\ s.t. \begin{cases} 105mm \le A \le 135mm \\ 0.5m/s \le B \le 1.1m/s \\ 15° \le C \le 25° \end{cases} \end{cases} \quad \text{(Eq. 5)}$$

According to the results of the simulation test, it can be seen that the width of the digging shovel, the angle of entry and the forward speed of the machine together affect the resistance generated when digging, through the optimization of the solution, it can be seen that when the width of the single shovel is 135 mm, the angle of entry is 20 °, and the forward speed of 0.5 m/s, the digging shovel is subject to the minimum resistance.

Analysis of field experiment

Figures 9-11 show the resistance curves generated by the vole-imitating digging shovel, gryllotalpa-imitating digging shovel and common digging shovel when advancing at forward speeds of 0.5 m/s, 0.8 m/s and 1.1 m/s, respectively, at different angles of entry.

The digging resistance of all three types of digging shovels at different entry angles increases with the forward speed, which is in accordance with the results of the simulation tests. The resistance fluctuations of the gryllotalpa-imitating digging shovel and the common digging shovel are more drastic than the simulation results because the actual operating conditions are more complicated, the soil distribution uniformity is lower than the discrete element model, and there are rocks, slabs, weeds, and other impurities in the ridge, so the consistency of the digging resistance is reduced. Under the same conditions, the resistance of the vole-imitating digging shovel is lower than that of the gryllotalpa-imitating digging shovel and common digging shovel, and the fluctuation amplitude of the resistance is larger than that of the gryllotalpa-imitating digging shovel and common digging shovel, which is in line with the results of the simulation and comparison test. The three types of digging shovels all produce the lowest resistance when digging under the working parameters of 20°angle of entry and 0.5 m/s forward speed, at which time the resistance of a single vole-imitating digging shovel is 174.53 N; the resistance of a single gryllotalpa-imitating digging shovel is 189.21 N; and the resistance of a single ordinary digging shovel is 212.59 N. The resistance reduction rate of the vole-imitating digging shovel is 17.91%, and that of gryllotalpa-imitating digging is 10.99%,

which is better than the resistance reduction performance of the vole-imitating digging shovel. The drag reduction rate was 17.91% for the vole-imitating digging shovel and 10.99% for the gryllotalpa-imitating digging, and the drag reduction performance of the vole-imitating digging shovel was better. In order to observe the crushing of soil on the shovel surface of the digging shovels in actual harvesting, the process of digging soil with three types of digging shovels was captured using the Intel D435 depth camera with the resolution selected to be 1920×1080 and the frame rate selected to be 30 fps. The pictures of the soil that was just passed into the conveyor belt after digging by different digging shovels were intercepted, as shown in FIG.12. By observing the broken state of the soil after digging with different digging shovels, the digging crushing ability of the three types of digging shovels is analyzed.

Analyzing the local zoomed image, it can be seen that there are almost no soil clods in the soil excavated by the vole-imitating digging shovel, which indicates that it has a better soil breaking effect, and the excavated soil is almost not bonded together; there are smaller soil clods in the soil excavated by the gryllotalpa-imitating digging shovel, which indicates that it has a certain soil breaking effect, and only a small portion of excavated soil is bonded together; and there are larger soil clods in the soil excavated by the common digging shovel, which indicates that its soil breaking effect is poor, and most of excavated soil is still bonded together. The larger clods in the soil excavated by the ordinary shovel indicate that it is less effective in breaking up the soil, and most of the excavated soil is still bonded together.

Conclusions

In this paper, a bionic vole-imitating digging shovel was designed based on the contour curve of the vole's paw-toe. The resistance-reduction performance of the vole-imitating digging shovel was explored through the incorporation of theoretical analysis and simulations. The following conclusions can be drawn from the above study:

i) Under the same simulation conditions, the vole-imitating digging shovel has the best crushing effect on soil particles and the lowest digging resistance, and its drag reduction rate is 21.64%, which is 9.56% higher than the gryllotalpa-imitating digging shovel. The digging resistance of the vole-imitating digging shovel will increase with the increase of shovel width and forward speed with a moderate entry angle (≥20°). Key influencing factors order followed: forward speed ＞ single shovel width ＞ entry angle, the optimal parameters combination

followed: single shovel width 135 mm, entry angle 20° and forward speed 0.5 m/s.

ii) In the field test, when the angle of entry is 20° and the forward speed is 0.5 m/s, the vole-imitating digging shovel produces the highest soil fragmentation degree and the lowest resistance, and the resistance reduction rate is 17.91%, which is 6.92% higher than that of the gryllotalpa-imitating digging shovel.

However, the resistance of the proposed vole-imitating digging shovel fluctuates greatly, and it still needs to be further optimized to improve its effectiveness and practicality.

Nomenclature:

η the drag reduction ratio of the bionic digging shovel, %;

F_v the resistance generated by the common digging shovel when digging, N;

F_u the resistance generated by the bionic digging shovel when digging, N;

References

Bayboboev, N., Muxamedov, J., Goyipov, U., Akbarov, S.B. 2022. Design of small potato diggers. IOP Conf. Ser. Earth Environ. Sci. 1010:012080.

Chengmao, C., Zhongbin, L., Wuyang, D., Manyu, W., Xuechen, Z., Kuan, Q. 2023. [Design and experiment of Ning-guo Radix peucedani bionic digging shovel].[Article in Chinese with English Abstract]. T. Chin. Soc. Agr. Machin. 54:102-113.

Chongchong, L., Lulu, X., Wujian, P. 2020. [Design and finite element analysis of bionic excavating shovel for Panax notoginseng seedlings].[Article in Chinese with English Abstract]. J. Chin. Agric. Mechan. 41:88-94.

Dassault Systèmes, 2022. SolidWorks (Version 2022) [Computer software]. Available from: https://www.solidworks.com

Dou, Q., Sun, Y., Sun, Y., Shen, J., Li, Q. 2019. [Current situation and development of potato harvesting machinery at home and abroad].[Article in Chinese with English Abstract]. J. Chin. Agric. Mechaniz. 40:206-210.

EDEM Ltd. 2020. EDEM (Version 2020.0) [Computer software]. Altair Engineering. Available from: https://www.altair.com/edem/

Gao, J., Jin, Z., Ai, A. 2024. The optimized design of soil-touching parts of a greenhouse humanoid weeding shovel based on strain sensing and DEM-ADAMS coupling simulation. Sensors (Basel) 24:868.

Gholamhossein, S., John, F., Jacky, D., Chris, S. 2010. Optimising oscillation frequency in oscillatory tillage. Soil Till. Res. 106:202-210.

Liang, Z., Huang, Y., Li, D., Wada, M.E. 2023. Parameter determination of a viscoelastic–plastic contact model for potatoes during transient collisions. Biosyst. Eng. 234:156-171.

Li, J.W., Tong, J., Hu, B., Wang, H.B., Mao, C.Y., Ma, Y.H. 2019. Calibration of parameters of interaction between clayey black soil with different moisture content and soil-engaging component in northeast China. T. CSAE 35:130-140.

MathWorks. 2020. MATLAB (Version 9.8.0.1451342 R2020a) [Computer software]. Available from: https://www.mathworks.com

Qishuo, D., Jun, R., Adam, B.E., Jikun, Z., Shuangyang, G., Yang, L. 2017. [DEM analysis of subsoiling process in wet clayey paddy soil].[Article in Chinese with English Abstract]. T. Chin. Soc. Agric. Machin. 48:38-48.

Shi, L.R., Sun, W., Wang, D., Zhao, W.Y., Liu, Q.W., Zhang, H., Wu, J.M. 2014. Design and simulation research on the potato bionic digging shovel. Agric. Res. Arid Areas 32:268-272.

Shi, L.R., Zhao, W.Y., Sun, W., Sun, B.G., Zhang, H. 2018. Research on the drag reduction performance of potato bionic digging shovel. Agric. Res. Arid Areas 36:286-291.

Stat-Ease, Inc. 2020. Design-Expert® (Version 13.0.7) [Computer software]. Available from: https://www.statease.com

Sun, W., Wang, H., Zhao, W., Zhang, H., Liu, X., Wu, J. 2018. [Design and experiment of potato digger with waste film recollection for complete film mulching, soil covering and ridge sowing pattern].[Article in Chinese with English Abstract]. T. Chin. Soc. Agric. Machin. 49:105-114.

Tunio, M.H., Gao, J., Shaikh, S.A., Lakhiar, I.A., Qureshi, W.A., Solangi, K.A., Chandio, F.A. 2020. Potato production in aeroponics: An emerging food growing system in sustainable agriculture for food security. Chil. J. Agr. Res. 80:118-132.

Wang, S., Li, S., Zhang, Y., Wan, Q., Chen, H., Meng, L. 2019. Mole toe bionics and surface heat treatment improving resistance reduction and abrasion resistance performance of toothed ditching blade. T. CSAE 35:10-20.

Wang, X., Fang, W., Han, D., Chen, X. 2022. Review of the research on soil disturbance by tools. Appl. Sci. 13:338.

Wan, X.x., Yang, W.j., Zhou, S.y., Su, H., Jiang, X., Dong, S.p., Jin, Z.-m. 2022. Comparative study on limb bones of four common rodents in Mudanjiang City. Hubei Agric. Sci. 61:102.

Wu, Y., Zhang, J., Hu, X., Huang, X., Zhang, X., Zou, X., Shi, J. 2023. A visible colorimetric sensor array based on chemo-responsive dyes and chemometric algorithms for real-time potato quality monitoring systems. Food Chem. 405:134717.

Xianliang, W., Hong, H., Qingjie, W., Hongwen, L., Jin, H., Wanzhi, C. 2017. [Calibration method of soil contact characteristic parameters based on DEM theory].[Article in Chinese with English Abstract]. T. Chin. Soc. Agric. Machin. 48:78-85.

Yang, L., Li, J., Lai, Q., Zhao, L., Li, J., Zeng, R., Zhang, Z. 2024. Discrete element contact model and parameter calibration for clayey soil particles in the Southwest hill and mountain region. J. Terramechanics 111:73-87.

Yang, R., Shang, S. 2012. Design and test of multifunctional curved-surface shovel in digging harvest. T. CSAE 28:47-52.

Yan, Z., Wilkinson, S.K., Stitt, E.H., Marigo, M. 2015. Discrete element modelling (DEM) input parameters: understanding their impact on model predictions using statistical analysis. Comput. Part. Mechan. 2:283-299.

Yu, J., Ma, Y., Wang, S., Xu, Z., Liu, X., Wang, H., et al. 2022. 3D finite element simulation and experimental validation of a mole rat's digit in-spired biomimetic potato digging shovel. Appl. Sci. 12:1761.

Zhang, Z., Xue, H., Wang, Y., Xie, K., Deng, Y. 2022. [Design and experiment of Panax notoginseng bionic excavating shovel based on EDEM].[Article in Chinese with English Abstract]. T. Chin. Soc. Agric. Machin. 53:100-111.

Zihui, L., Xinyu, W., Jinqing, L., Jicheng, L., Shujuan, Y., Dan, Q. 2019. [Analysis and prospect of research progress on key technologies and equipments of mechanization of potato planting].[Article in Chinese with English Abstract]. T. Chin. Soc. Agric. Machin. 50:1-16.

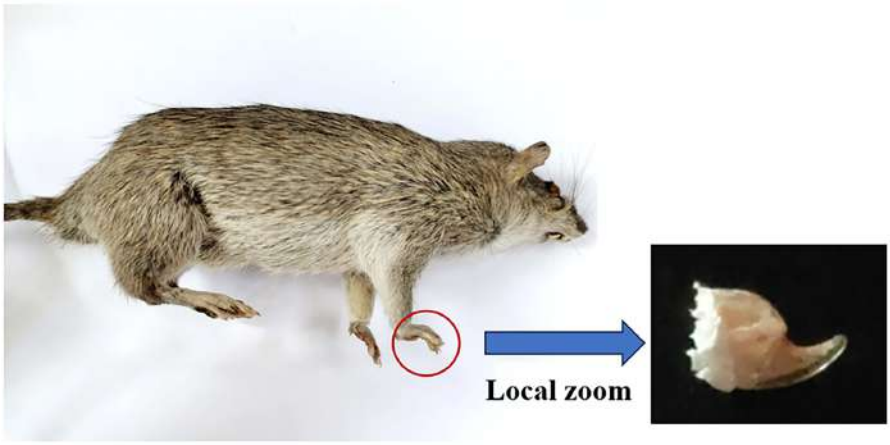

Figure 1. Paw and toe information extraction in voles.

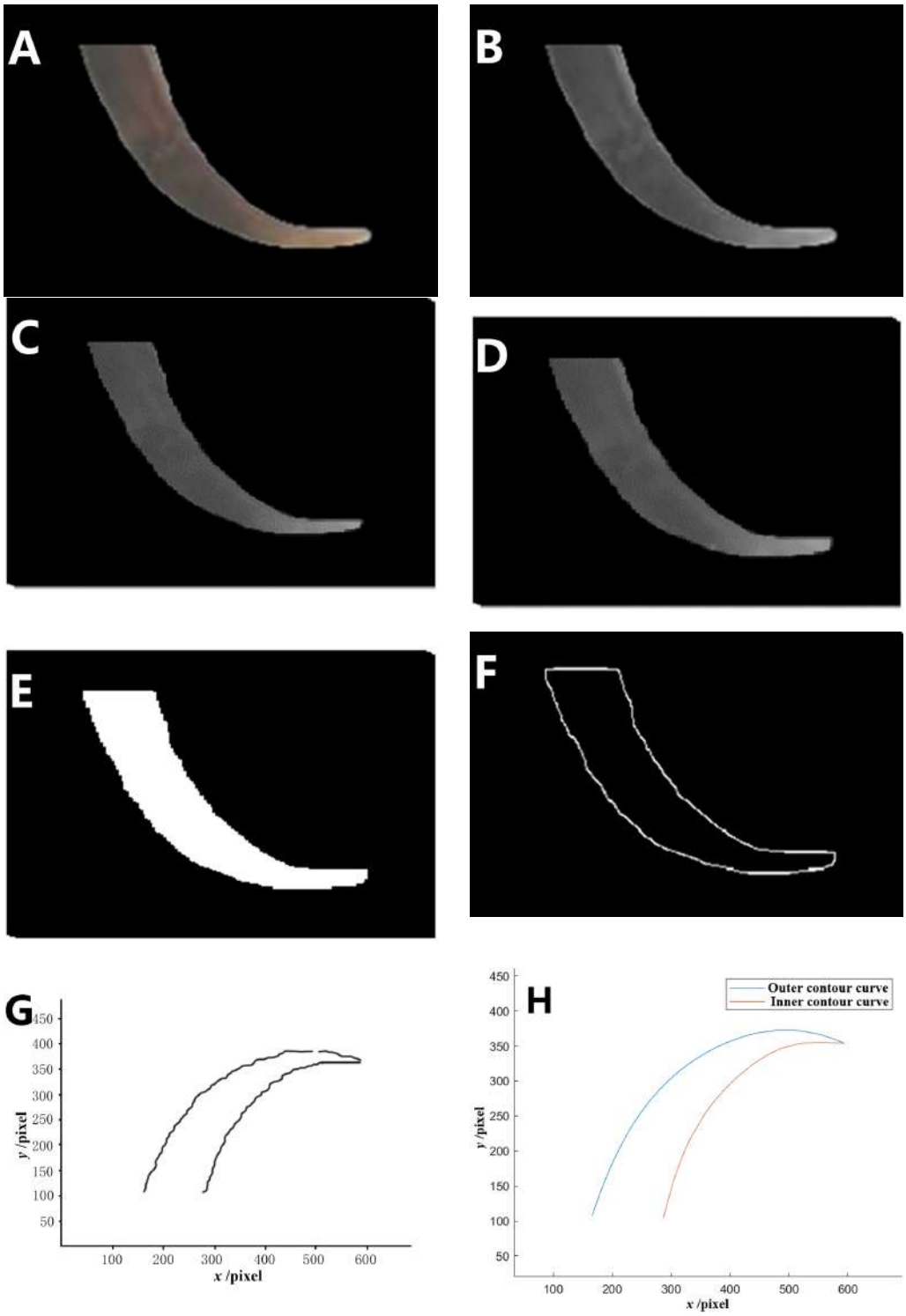

Figure 2. Flowchart of image processing of front middle toe of the vole: (A) Original image; (B) Grayscale processed image; (C) Eroded image; (D) Expanded image; (E) Binarized image; (F) Profile curve; (G) The lateral contour curves of the front middle toe of the vole; (H) The fitted contour curves of the front middle toe of the vole.

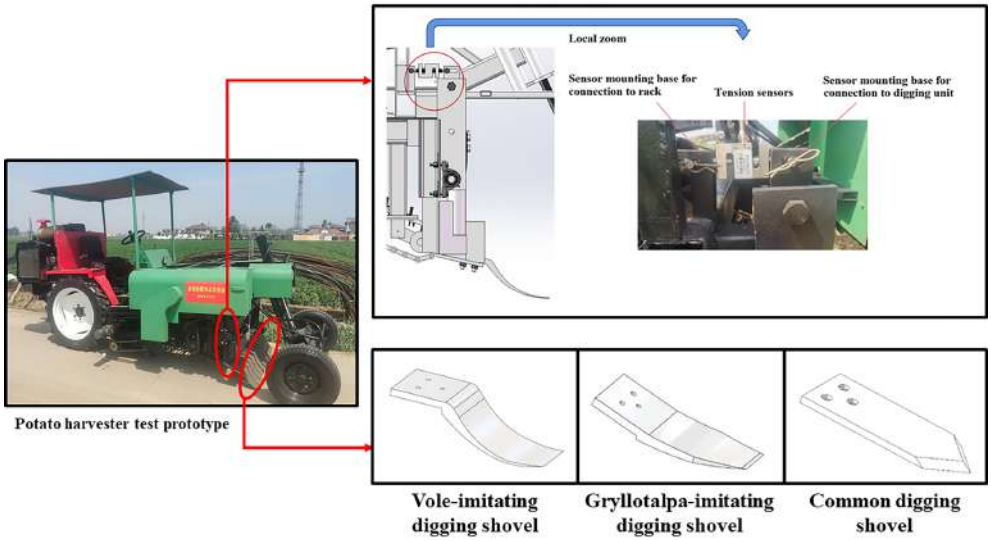

Figure 3. Potato harvester test prototype with digging resistance test system and three types of digging shovels.

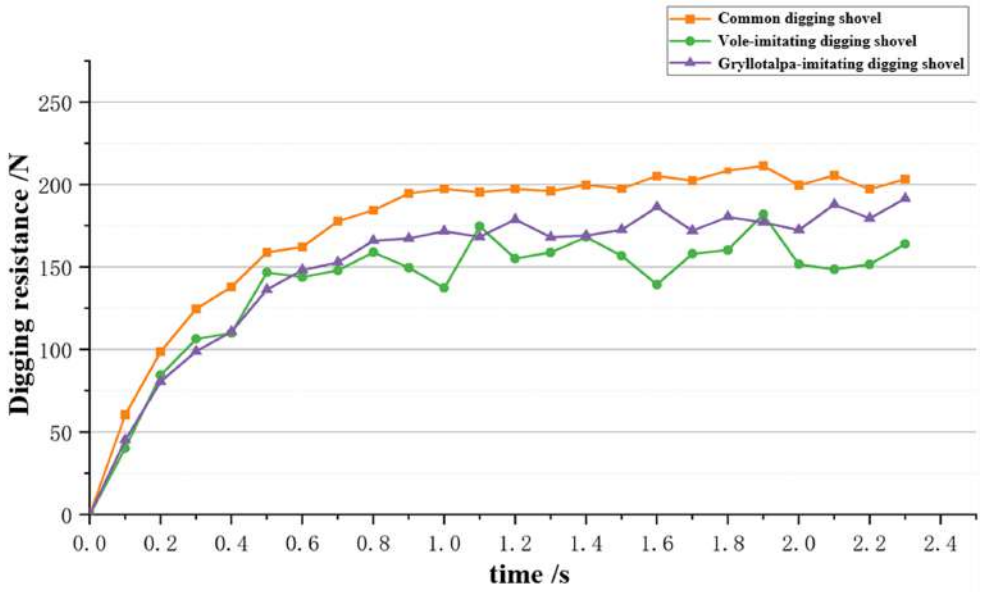

Figure 4. Comparison Curve Chart of resistance generated by the three types of digging shovels.

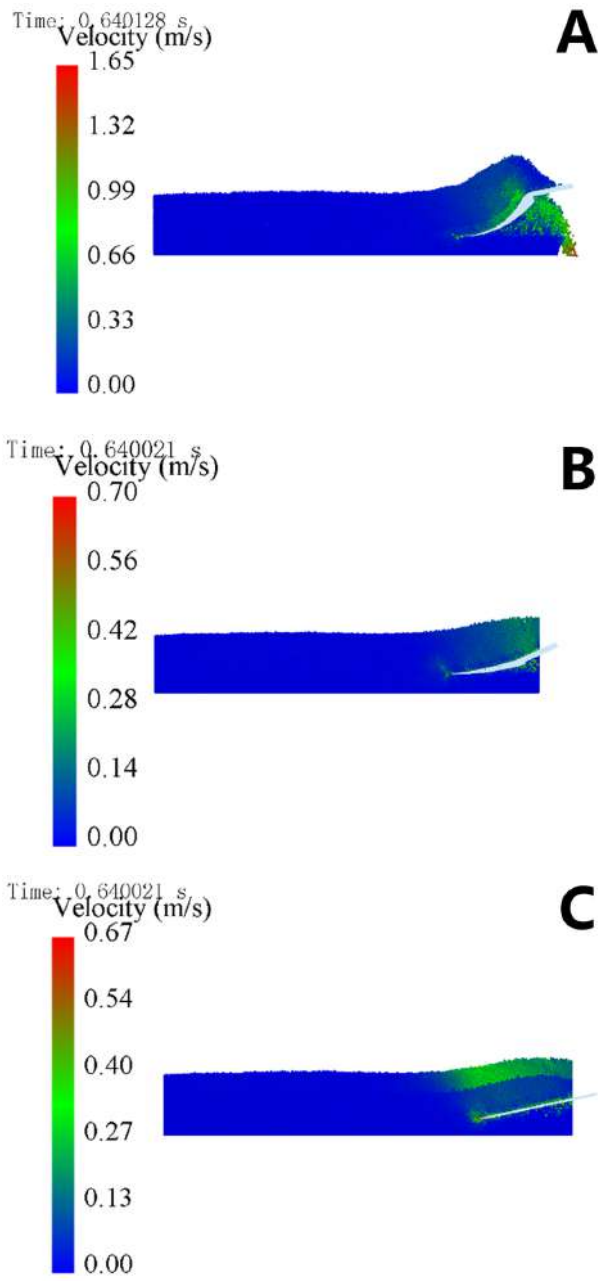

Figure 6. Comparison of soil particle velocity changes at the shovel face of three types of digging shovels: (A) vole-imitating digging shovel; (B) gryllotalpa-imitating digging shovel; (C) common digging shovel.

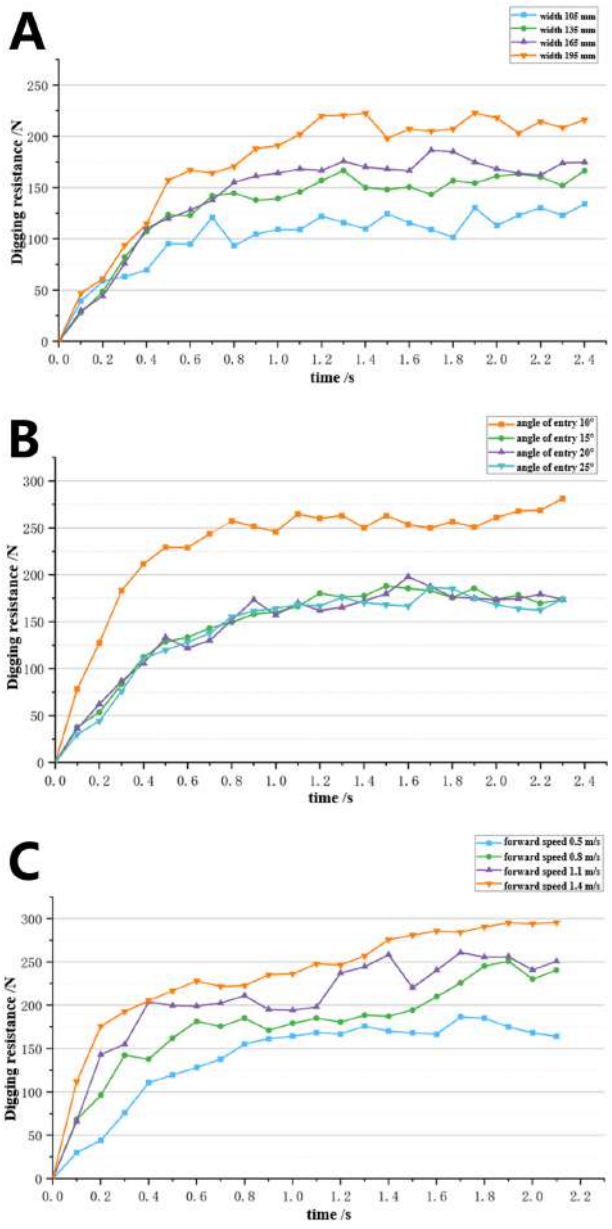

Figure 7. One-factor simulation test of digging resistance change: (A) Effect of shovel width on digging resistance; (B) Effect of angle of entry on digging resistance; (C) Effect of forward speed on digging resistance.

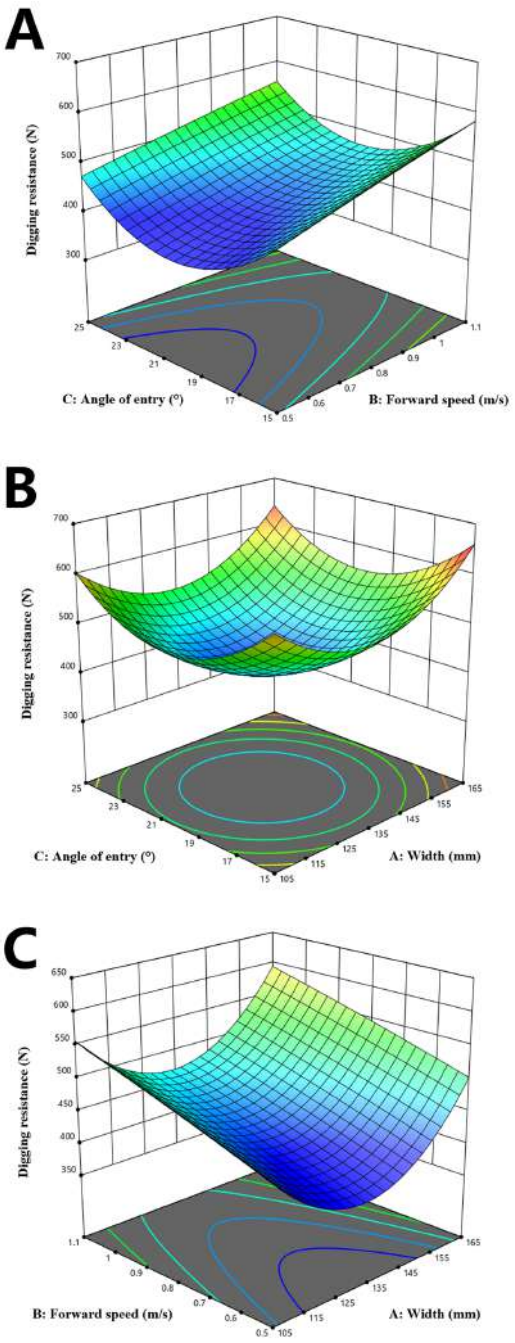

Figure 8. Response surface diagram: (A) Effect of B and C on digging resistance for A=135 mm; (B) Effect of A and C on digging resistance for B = 0.8 m/s; (C) Effect of A and B on digging resistance at C = 20°.

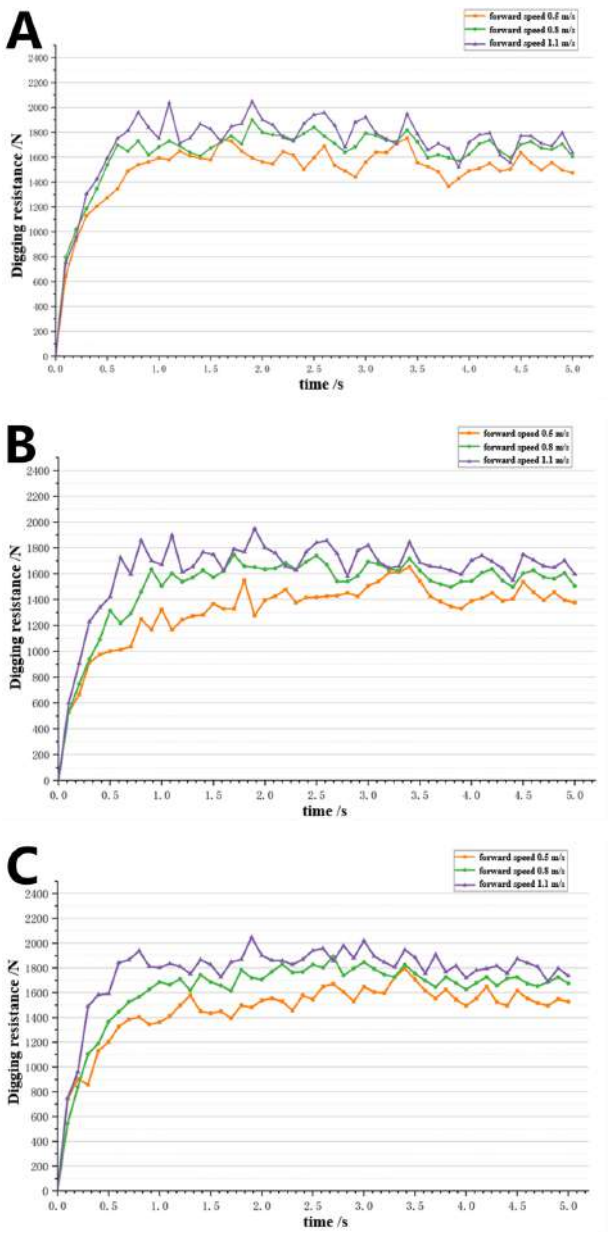

Figure 9. Vole-imitating digging shovel resistance curve: (A) The angle of entry is 15°; (B) The angle of entry is 20°; (C) The angle of entry is 25°.

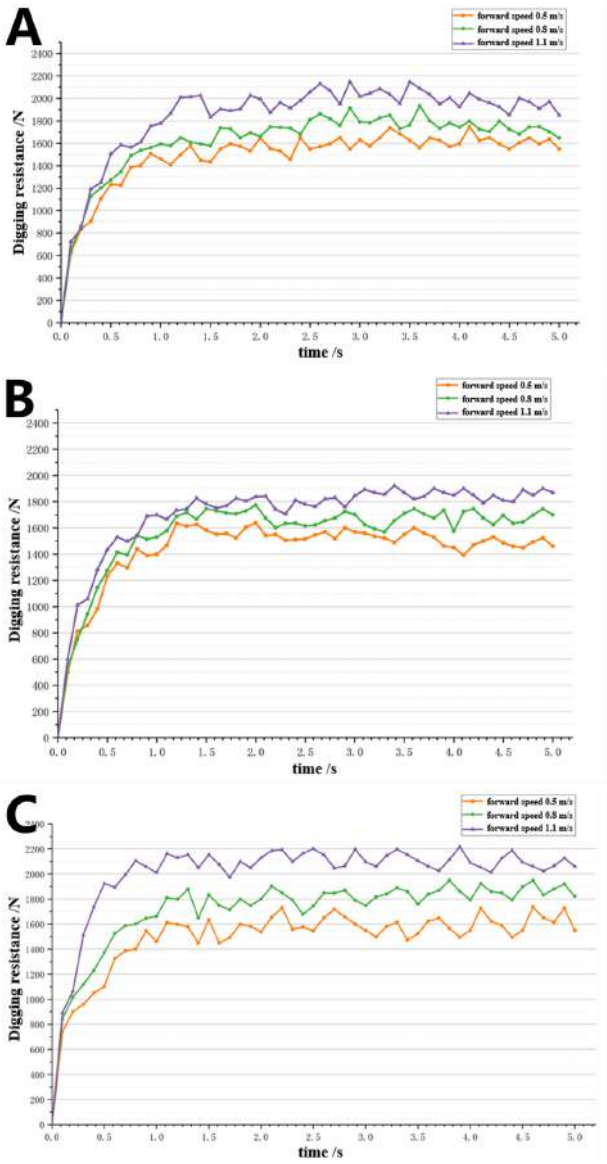

Figure 10. Gryllotalpa-imitating digging shovel resistance curve: (A) The angle of entry is 15°; (B) The angle of entry is 20°; (C) The angle of entry is 25°.

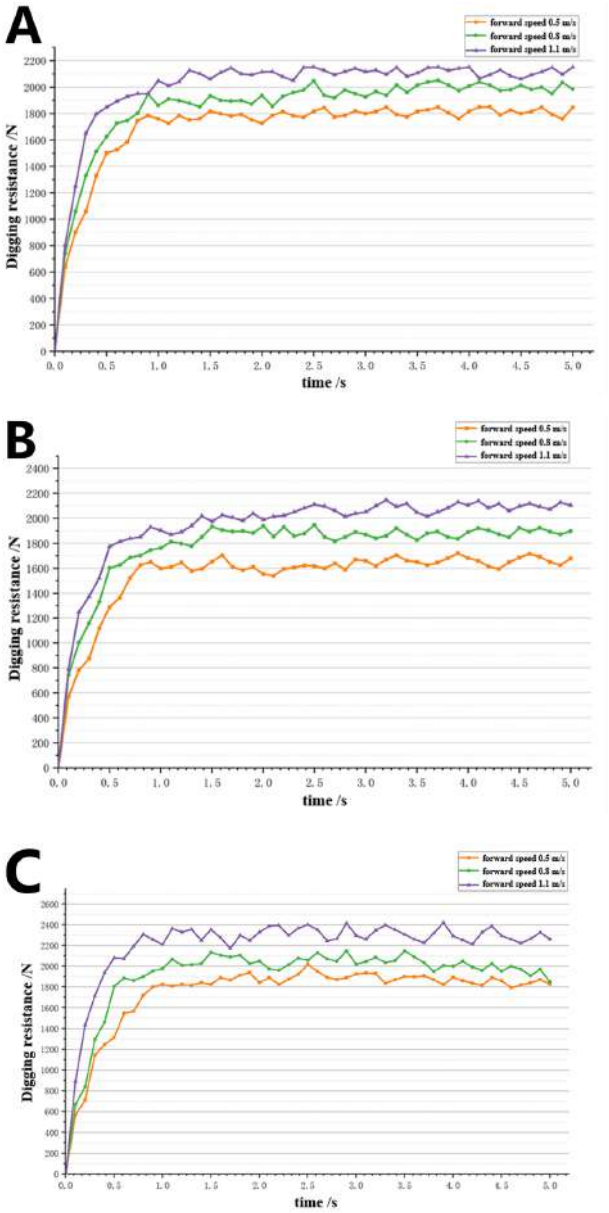

Figure 11. Common digging shovel resistance curve: (A) The angle of entry is 15°; (B) The angle of entry is 20°; (C) The angle of entry is 25°.

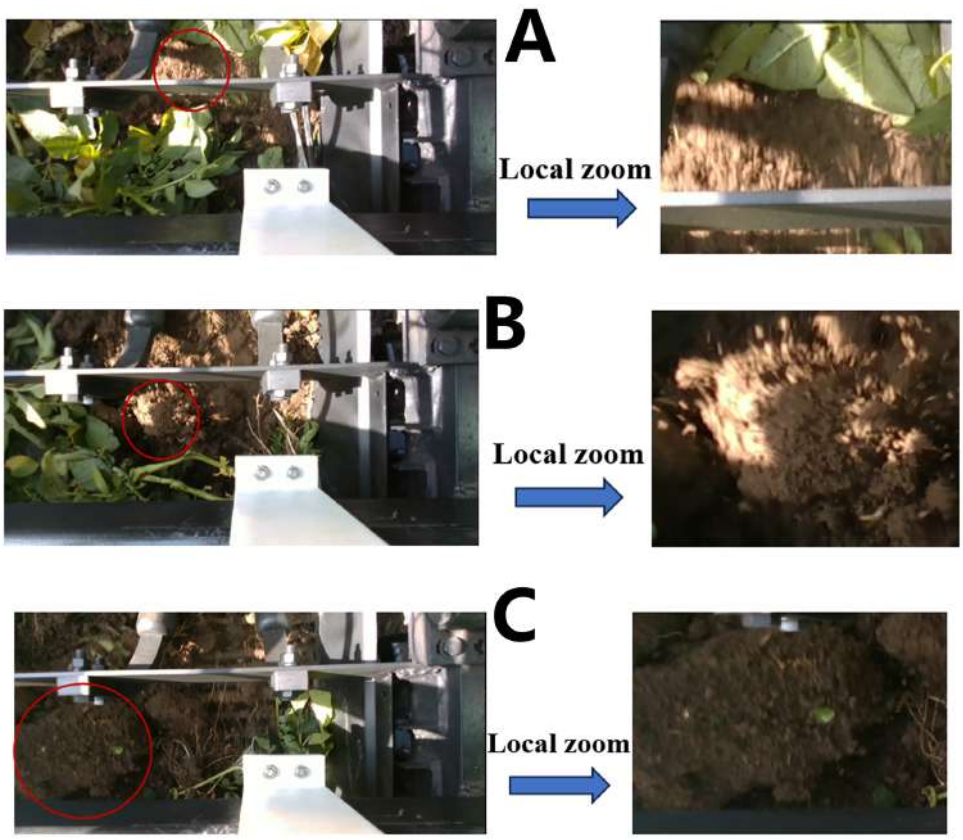

Figure 12. Comparison of soil fragmentation on the surface of three types of digging shovels: (A) Vole-imitating digging shovel; (B) Gryllotalpa-imitating digging shovel; (C) Common digging shovel.

Table 1. Basic parameter settings of soil and digging shovel.

Material parameter	Symbol	Value
Poisson ratio of soil	/	0.3
Density of soil	g/cm^3	1.23
Shear modulus of soil	Pa	1×106
65MnPoisson Ratio of soil	/	0.3
65Mn Density of soil	g/cm^3	7.85
65Mn Shear modulus of soil	Pa	7.86×1010
Recovery coefficient (soil to soil)	/	0.3
Static friction coefficient (soil to soil)	/	0.5
Friction coefficient (soil to soil)	/	0.2
Recovery coefficient (soil to shovel)	/	0.3
Static friction coefficient (soil to shovel)	/	0.3
Friction coefficient (soil to shovel)	/	0.1

Table 2. One-factor simulation test arrangement.

Test number	Factor		
	Single shovel width A (mm)	Forward speed B (m/s)	Angle of entry C (°)
1	105	0.5	20
2	135		
3	165		
4	195		
5	165	0.5	20
6		0.8	
7		1.1	
8		1.4	
9	165	0.5	10
10			15
11			20
12			25

Table 3. Results of multifactorial simulation tests.

Number	Factor			c(N)
	Single shovel width A (mm)	Forward speed B (m/s)	Angle of entry C (°)	
1	165	0.8	25	647.809
2	105	1.1	20	561.763
3	135	1.1	25	541.861
4	135	0.8	20	458.032
5	135	0.5	25	469.85
6	105	0.8	25	616.064
7	165	0.8	15	648.548
8	165	0.5	20	498.019
9	135	0.8	20	419.161
10	165	1.1	20	602.128
11	135	1.1	15	588.05
12	105	0.5	20	447.486
13	105	0.8	15	604.95
14	135	0.8	20	423.388
15	135	0.8	20	411.102
16	135	0.8	20	415.949
17	135	0.5	15	491.016

Table 4. Analysis of variance for digging resistance.

Source	Square sum	Degrees of freedom	Mean square sum	F-value	Significant *p*-level
Model	1.155E+05	9	12837.09	36.07	<0.0001
A	3454.51	1	3454.51	9.71	0.0169
B	18762.85	1	18762.85	52.72	0.0002
C	405.84	1	405.84	1.14	0.3210
AB	25.85	1	25.85	0.0726	0.7953
AC	35.12	1	35.12	0.0987	0.7626
BC	156.54	1	156.54	0.4398	0.5284
A2	45747.58	1	45747.58	128.54	<0.0001
B2	24.52	1	24.52	0.0689	0.80051
C2	41752.99	1	41752.99	117.32	<0.000
Residual	2491.3	7	355.90		
Lost proposal	1089.81	3	363.27	1.04	0.4665
Inaccuracy	1401.5	4	350.37		